Ceramics International 51 (2025) 64146–64157

Contents lists available at ScienceDirect

Ceramics International

journal homepage: www.elsevier.com/locate/ceramint

Photoluminescence and structure of Sm^{3+} activated magnesium–borate glasses for lighting applications

A. Samir [a,*], M. Farouk [b,**], M. Attallah [c,d,***]

[a] Basic Science Department, Faculty of Engineering at Shoubra, Benha University, Cairo, 11629, Egypt
[b] Physics Department, Faculty of Science, Al–Azhar University, Nasr City, Cairo, 11884, Egypt
[c] Basic Science Department, Higher Technological Institute, 10th of Ramadan City, Egypt
[d] Faculty of Engineering, City University of Cairo (CUC), New Heliopolis City, Cairo, Egypt

ARTICLE INFO

Handling Editor: P. Vincenzini

Keywords:
Photoluminescence
Sm^{3+} ion
CIE diagram
FT-IR
Orange phosphors
Metallization

ABSTRACT

A series of Sm^{3+}-doped Na_2O–ZnO–MgO–B_2O_3 glasses was synthesized by melt-quenching techniques. X-ray diffraction confirmed the amorphous (non-crystalline) nature of the glassy systems. The impact of Sm_2O_3 concentration on the physical, structural, and optical properties was investigated. Both molar volume and density exhibit a positive correlation, indicating an upward trend. The structural change correlated with an increase in density and molar volume. FT-IR spectroscopy demonstrated the transmutation of BO_4 units to BO_3 units as the content of Sm_2O_3 increased, resulting in a rise in non-bridging oxygens (NBOs). The optical band gap (E_{opt}) decreased from 3.39 eV to 2.71 eV as the Sm^{3+} content increased, indicating an escalation in disorder within the glass network. Under 403 nm excitation, the photoluminescence spectra exhibited four intense emission peaks at 562, 598, 646, and 709 nm, corresponding to the $^4G_{5/2} \rightarrow {}^6H_{5/2}$, $^6H_{7/2}$, $^6H_{9/2}$, and $^6H_{11/2}$ transitions of Sm^{3+} ions, respectively. The prominent orange-red emission at 598 nm ($^4G_{5/2} \rightarrow {}^6H_{7/2}$) was the most significant feature. The CIE chromaticity coordinates indicated a brilliant reddish-orange emission, with CCT within the warm-light spectrum 1860–2759 K. The synthesized Sm^{3+}-doped borate glasses are promising candidates for orange-red-emitting solid-state lighting and photonic applications.

1. Introduction

B_2O_3 glasses exhibit several notable characteristics, including high visible-range luminescence efficiency, robust glass-forming ability, exceptional optical transparency, excellent solubility in rare-earth elements, and cost-effective manufacturing. Borate glasses also feature a convoluted three-dimensional structure of boron and oxygen. Modifier ions, including alkali and transition metal oxides, locally modify the glass network. These changes influence chemical stability, bond energies, and structural groupings. The dielectric properties of borate glasses are essential for optimizing their composition to achieve desired outcomes, including a low loss tangent, a high dielectric constant, and accurate refractive indices. It also possesses two distinct coordination environments for boron atoms, rendering it more fascinating than other host materials. Due to these factors, research into the photonic applications of doped borate glasses and their luminescence characteristics is crucial for developing advanced optical devices and sensors. It is feasible to optimize the composition of B_2O_3 glasses to enhance their performance in photonic applications by understanding the underlying mechanisms that control their luminescent properties. The only significant drawback of B_2O_3 is its high phonon energies (1300 cm^{-1}). It is possible to enhance the host material's radiation–emitting capabilities and reduce the excess phonon energy of borates by adding an appropriate glass modifier [1–6].

One approach to enhancing the stability of borate-based glasses is to incorporate additional metal oxides, such as magnesium oxide (MgO), as network modifiers. That is because MgO forms a B−O−M network, which is highly resistant to hydrolysis by air. MgO is included in the glass composition as a modifier to enhance chemical durability, hardness, and mechanical strength. Moreover, it reduces the phonon energy

* Corresponding author.
** Corresponding author.
*** Corresponding author. Basic Science Department, Higher Technological Institute, 10th of Ramadan City, Egypt.
E-mail addresses: ahmed.soliman01@feng.bu.edu.eg (A. Samir), m_Farouk@azhar.edu.eg, mf_egypt22375@yahoo.com (M. Farouk), m_attallah94@yahoo.com, mohamed.atallh@hti.edu.eg (M. Attallah).

https://doi.org/10.1016/j.ceramint.2025.11.152
Received 7 August 2025; Received in revised form 7 November 2025; Accepted 11 November 2025
Available online 12 November 2025

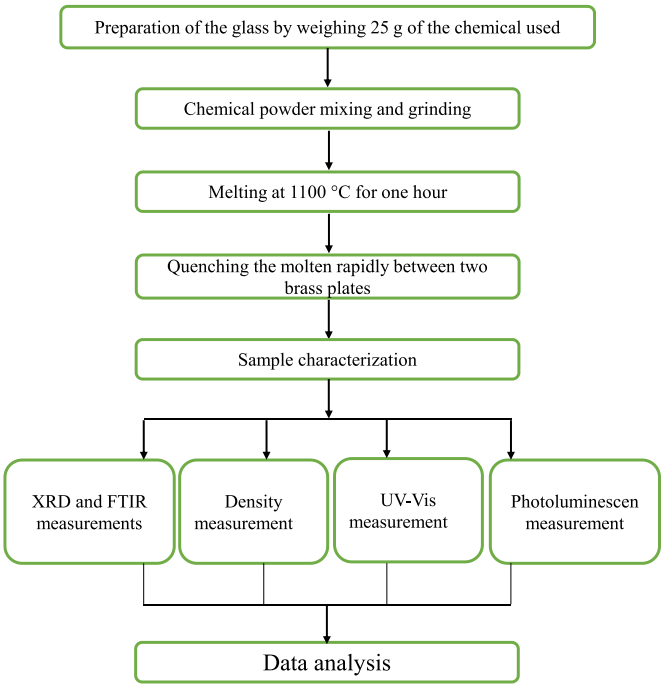

Fig. 1. Flow chart of the fabrication process and measurements used for the study of the investigated glass system.

and brittleness of the glass [7–10]. The addition of sodium oxides enhances borate glass by increasing the solubility of rare earth ions and lowering its melting point. In optics and materials science, borate glass is an emerging topic that warrants further exploration. Its adaptability and distinctive characteristics render it a prospective candidate for various applications, including communications and nonlinear devices [11,12].

ZnO ingresses into the glass matrix in two forms: network formation and modification. As a network modifier, ZnO improves electrical, magnetic, and optical properties due to its broad band-gap, high exciton binding energy, ability to withstand high humidity, and intrinsic emission features. As a result, it is appropriate for the production of optical components, solar energy converters, optoelectronic devices, and UV-emitting lasers. Particularly noteworthy properties of borate glasses containing zinc include high thermal stability, polarizability, insulating strength, chemical durability, and superior optical transparency across a wide range of wavelengths [4,13–15].

One of the best-performing lanthanide ions, exhibiting various advantageous properties in glasses, is the Sm^{3+} ion. It includes down-conversion, an activator function, and excellent quantum efficiency, resulting from its high optical band gap, long-serving lifetime, and effective fluorescence. Sm_2O_3 glasses have a more comprehensive spectral range, extending from the ultraviolet to the infrared. This extended range has several applications in optoelectronics, and its superior red-orange emissions have facilitated the development of solid-state lasers, photovoltaic devices, colour displays, medical imaging, optical amplifiers, optical fiber communications, optical memory devices, and temperature sensors [16–22]. Beyond the other features of the Sm^{3+} ion, the luminescence center exhibits three transition emission bands: roughly 565, 602, and 650 nm, corresponding to yellow, orange-red, and red light, respectively. The reddish-orange light emitted by Sm^{3+} activated glasses is attributed to transitions from $^4G_{5/2} \rightarrow {}^6H_{5/2}$, $^6H_{7/2}$, $^6H_{9/2}$, and $^6H_{11/2}$, with the $^4G_{5/2} \rightarrow {}^6H_{7/2}$ transition being hypersensitive. Compared to borate glasses, the substantial energy difference (7400 cm^{-1}) between the $^4G_{5/2}$ and $^6H_{11/2}$ levels reduces multi–phonon transmission rates, resulting in a host matrix with high quantitative efficiency and favourable emission characteristics. This emission benefits high-power lasers in optical waveguides and compact fibers [23–28].

The premier purpose of this research is to assess the efficacy of particular raw materials employed in producing alkali borate glass doped with Sm^{3+} ions. The physical, structural, and luminous characteristics of the glasses have been investigated to assess their suitability for applications involving orange-red lighting, solid-state lasers, and photonics.

2. Experimental methodology

2.1. Glass synthesis

A new series of trivalent samarium ions (Sm^{3+}) doped magnesium–sodium–zinc–borate glass for optoelectronic applications was prepared by the melt-quenching approach. Fig. 1 illustrates the characterization of the investigated samples. The chemical compositions of the samples are: [(60-x) B_2O_3 - 20Na_2O – 10ZnO – 10MgO – xSm_2O_3], x = zero, 0.5, 1.0, 1.5 and 2.0 mol%. High-purity (99.99 %) powders of

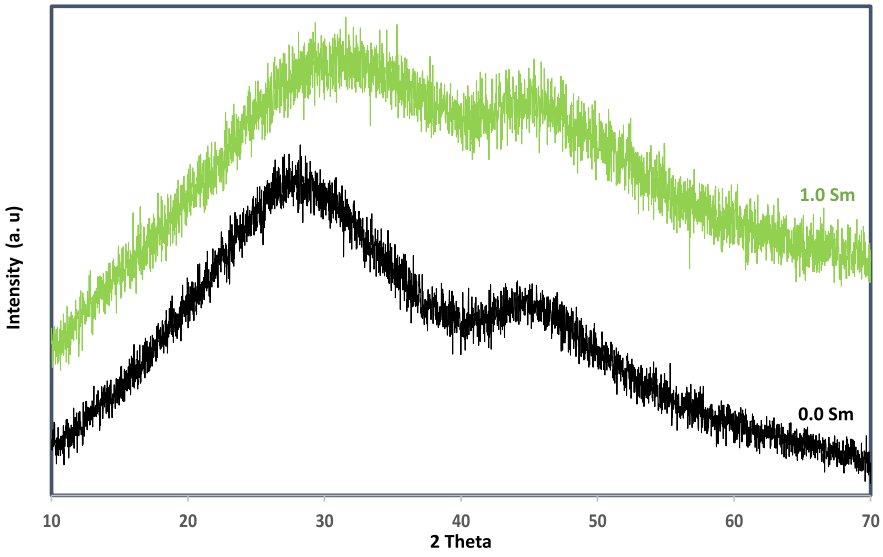

Fig. 2. XRD for the investigated glass system.

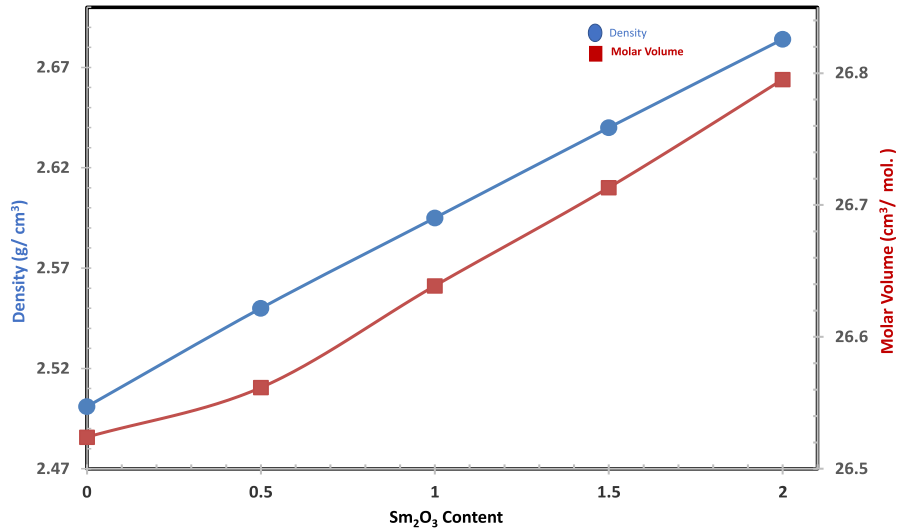

Fig. 3. Variation of density and molar volume against Sm_2O_3 Content.

H_3BO_3, MgO, ZnO, Na_2CO_3, and Sm_2O_3 were used as starting glass constituents. A batch of approximately 25 g was weighed. Each batch was mixed, placed in a porcelain crucible, and melted at 1100 °C for 60 min. To ensure the compounds were evenly distributed and that a bubble-free liquid was developed, the mixture was periodically agitated every 10 min. After achieving the desired viscosity, the melt mixture was rapidly cooled between two brass plates, annealed for 4 h at about 400 °C to lessen thermal stresses and breakage, and then allowed to cool to room temperature. The resultant samples were evident and thermally stable; therefore, they were employed for UV–Vis and photoluminescence measurements. Additionally, crushed samples were utilized for XRD (X-ray diffraction) and FT-IR (Fourier–transform infrared) analyses.

2.2. Sample characterization

An XRD analysis was performed on the powder to verify the amorphous nature of the glasses. The measurements were conducted using a Bruker-D8 Advance Diffractometer (Brüker, UK) at a rate of 0.050°/sec, with the scanning angle 2θ ranging from 10° to 80°. The conventional Archimedes approach utilized experimental density data, with carbon tetrachloride ($\rho = 1.595$ g/cm^3) as the immersion liquid. A portion of the powder from each sample was mixed with KBr, and the mixtures were then pressed to obtain homogeneous pellets. Subsequently, the existing vibrational groups were obtained by recording infrared spectra using a Nicolet iS50 FT–IR Spectrometer (Thermo Fisher Scientific) over the 1750–400 cm^{-1} range. The UV–Vis spectra were measured using a JASCO V–670 Spectrometer, covering a wavelength range of 200–1700 nm, to illustrate the optical characteristics. The 150-W Xenon arc lamp on the JASCO FP–6500 Spectrofluorometer is employed to acquire the system's excitation and emission spectra.

3. Results and discussion

3.1. XRD

XRD confirmed the amorphous nature of the glassy system, as illustrated in Fig. 2, with no sharp peaks in the examined samples [29].

3.2. Density and physical parameters

Density is a potent instrument for analyzing the structure of the glass sample. A multitude of factors influence it, including the distance between glass, crosslink density, coordination numbers, and geometric structure. The density measurements of the glasses under investigation were acquired. The following expression was used to get the glass density [30]:

$$\rho = \left[\frac{a}{a-b}\right]^{*}\rho_l \quad (1)$$

where a is the weight in the air and b is the weight in the carbon tetrachloride (liquid). The glasses' molar volumes (V_m) were calculated from their average molecular weights. As a result of this formula [31]:

$$V_m = \frac{M}{\rho} \quad (2)$$

where ρ denotes the sample's density, and M symbolizes its molecular weight. The fluctuation of ρ and V_m with the concentration of Sm^{3+} ions is illustrated in Fig. 3. The addition of Sm_2O_3 results in an increase in both the ρ and V_m values. The density increase is closely related to the molecular weights of the glass samples' constituents. Consequently, substituting Sm_2O_3 with B_2O_3 is expected to make the glass denser, as the molecular weight of Sm_2O_3 (348.72 g/mol) exceeds that of B_2O_3

Table 1
Density (ρ), molar volume (V_m), Sm^{3+} ions concentration (N_{Sm}), inter ionic distance (r_i), Polaron radius (r_p), Field strength (F), refractive index (n), oxygen packing density, optical band-gap (E), Urbach energy (ΔE) and Metallization (M) for the investigated samples for the investigated samples.

Sample (mol. %)	ρ (g/cm^3) ±0.001	V_m (cm^3/mol.) ±0.001	$N_{Sm} \times 10^{20}$ (ion/cm^3) ±0.001 × 10^{20}	ri (Å) ±0.001	r_p (Å) ±0.001	F × 10^{14} (cm^{-2}) ±0.001	n ±0.01	OPD (g-atom/l) ±0.001	E_g (eV)	ΔE (eV)	M
0.0 Sm	2.50	26.52	0	0	0	0	1.5	75.40	3.39	0.22	0.41
0.5 Sm	2.55	26.54	1.13	2.06	8.32	4.32	1.506	75.35	3.16	0.23	0.39
1.0 Sm	2.59	26.63	2.25	1.64	6.61	6.85	1.511	75.07	2.96	0.25	0.38
1.5 Sm	2.64	26.64	3.38	1.43	5.77	8.98	1.517	75.06	2.86	0.30	0.37
2.0 Sm	2.68	26.83	4.48	1.30	5.26	10.8	1.52	74.52	2.71	0.31	0.36

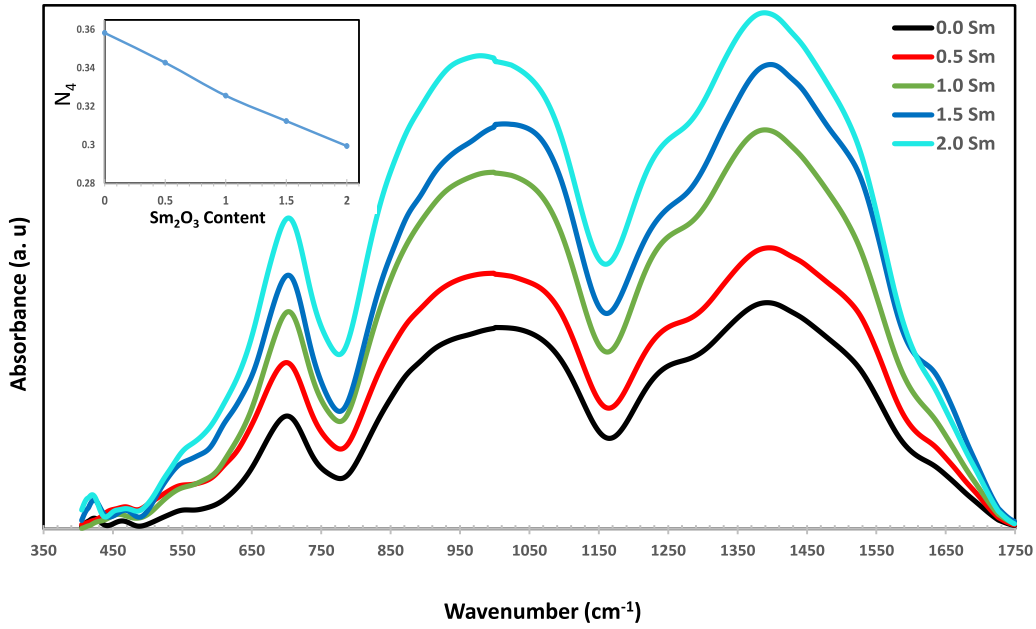

Fig. 4. Vibrational infrared spectra of the prepared glass samples, and the inset figure is for the variation of N_4.

(69.61 g/mol) [6]. When Sm_2O_3 is added, boosts in calculated molar volume are observed (Fig. 3). This is mainly because of the formation of NBOs with increasing Sm_2O_3 content, as later confirmed by FT-IR. Another possibility is attributed to the samarium ionic radius ($r = 1.079 \times 10^{-10}\ m$) is more extensive than boron's ($r = 0.27 \times 10^{-10}\ m$), the free volume is increased. The Sm^{3+} ions concentration, N, was determined using $(ion/cm^3) = \frac{x\rho N_A}{M_W}$, in which x represents the mole fraction of Sm^{3+}, whereas N_A denotes Avogadro's number. The interatomic distance r_i was calculated via $r_i = \left(\frac{1}{N}\right)^{1/3}$, polaron radius r_p by $r_p = \frac{1}{2}(\pi/6N)^{1/3}$, and the field strength F surrounding the Sm^{3+} ion by $F = \frac{Z}{r_p^2}$, where z is the valence of Sm^{3+} ion [32]. The values for the various physical properties of the samples under investigation are displayed in Table 1. It has been found that when Sm_2O_3 content increases, N also increases. This results in a decrease in the polaron radius and the interionic distance, which in turn causes the Sm–O distance to decrease. The field strength surrounding Samarium ions is enhanced as a result of the strengthening of the Sm–O bond. One of the optical parameters associated with the glassy material is its refractive index (n). The equation used to obtain the refractive index is [$n = \frac{\rho+10.4}{8.6}$] [33] where ρ is the density of the sample, Table 1 presents the values of n, which show an increase from 1.50 for the Samarium–free sample to 1.54. With the addition of Sm_2O_3, the refractive index (n) rises gradually. The chief cause of this increase, as evidenced by FT-IR measurements, is the formation of NBOs as a consequence of the breaking of glass network structures. Finally, the following relation can be used to

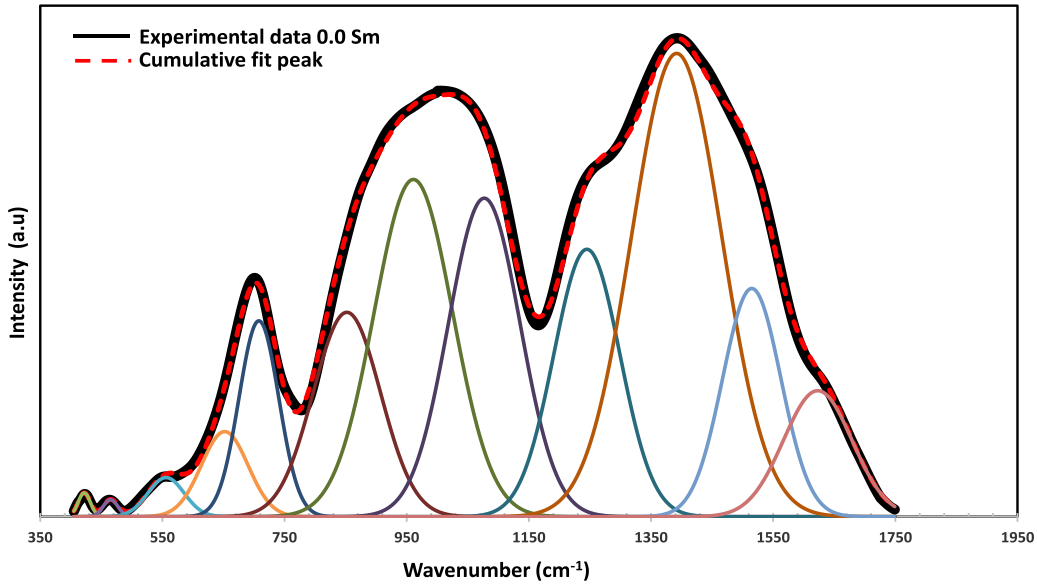

Fig. 5. A representative example (0.0 Sm) for the deconvolution process.

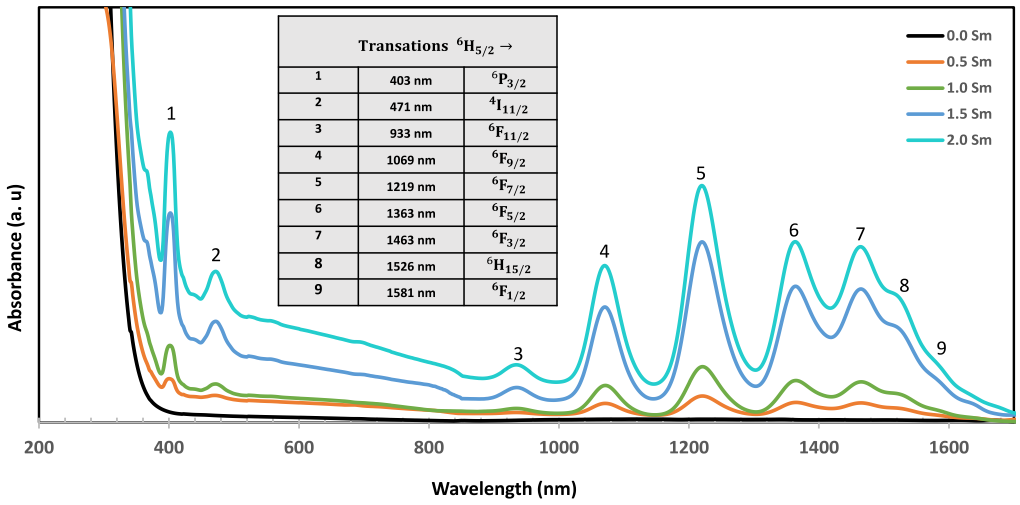

(a)

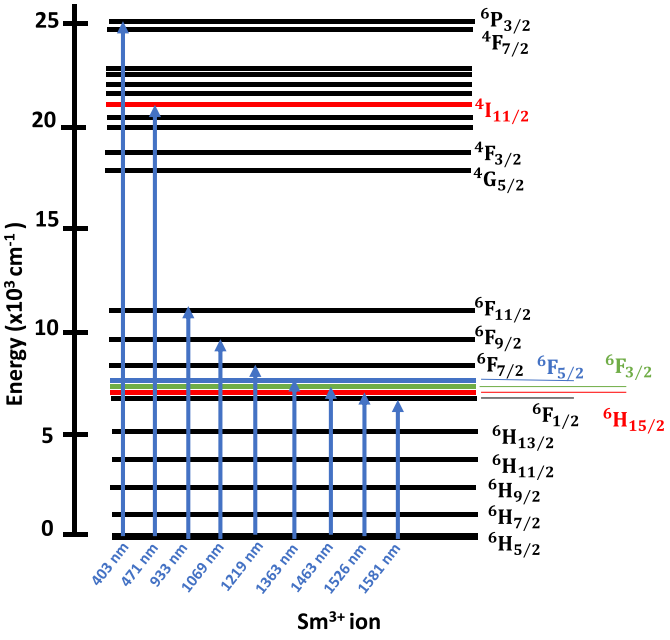

(b)

Fig. 6. (a and b). Absorption spectra and the corresponding transitions of the investigated samples.

compute oxygen packing density (OPD), [$OPD = \left(\frac{\rho}{M_W}\right)*n$], where the number of oxygen atoms in a formula unit is represented by n [34]. From the tabulated data in Table 1. As the amount of Sm_2O_3 content increases, the OPD decreases. In the analyzed glassy system, this indicates that an increase in Sm_2O_3 content results in a less densely packed structure (open structure), and an increase in disorder.

3.3. FT-IR analysis

Infrared spectroscopy was utilized to understand the conversion between borate groups (BO_3 and/or BO_4). Fig. 4 shows the infrared absorption spectra of the glass samples. Oscillations of borate groups are observed in the 600–1600 cm^{-1} wavenumber range [35]. The amorphous characteristic of the investigated samples results in the bands appearing exceptionally broad. Each spectrum was repeatedly deconvoluted into Gaussian profiles to ascertain the source of these unique bands. For example, Fig. 5 shows a sample containing 0.0 Sm. The cumulative fitting spectrum ensures that the experimental data are adequately fitted. Based on Fig. 4 and 5. A feeble band at ~422 cm^{-1} was observed, possibly due to Sodium ionic vibrations, Na^+– O [36,37]. Oxygen metal cations of O–Zn^{2+} and/or O–Mg^{2+} are to blame for the vibrational bands ~465 cm^{-1} [38]. The bending vibrations of B–O–B are responsible mainly for the band ~556 cm^{-1} [39]. The symmetrically O–B–O bending vibration band of the bridging oxygen in BO_3 corresponded to a band at ~652 cm^{-1} [12]. The band ~708 cm^{-1} is likely relevant to the vibrations of symmetric B–O–B bending in bridge oxygen in trigonal units [40]. The band at ~852 cm^{-1} is associated with B–O stretching vibrations of NBOs in BO_4 [41]. The bands ~961 cm^{-1} and 1077 cm^{-1} could be linked to vibrations that stretch B–O bonds and the rocking motion for BO_4 [42]. The prominent band ~1245 cm^{-1} is likely related to the symmetric stretching vibrations of B–O of NBOs in BO_3

Table 2
Transition states and their wavelength for the investigated samples.

Transitions from $^6H_{5/2}$→	Wavelength (nm)	Energy Sm^{3+} (cm^{-1})	Energy $_{(aq)}$ (cm^{-1})
$^6P_{3/2}$	403	24813	24999
$^4I_{11/2}$	471	21231	21096
$^6F_{11/2}$	933	10718	10517
$^6F_{9/2}$	1069	9354	9136
$^6F_{7/2}$	1219	8203	7977
$^6F_{5/2}$	1363	7336	7131
$^6F_{3/2}$	1463	6835	6641
$^6H_{15/2}$	1526	6553	6508
$^6F_{1/2}$	1581	6325	6397

[43]. The B–O asymmetric stretched vibrations of BO_3 are responsible for the conspicuous infrared absorption bands ~1392 and 1515 cm^{-1} [44,45]. The existence band ~1623 cm^{-1}, is overlapping with B O_3 band indicative of OH bending vibration [46]. One may use the following relation to estimate N_4 (four-coordinated boron). $N_4 = \left(\frac{A_4}{A_4+A_3}\right)$, where the areas of BO_3 bands and BO_4 bands are represented by the letters A_3 and A_4, respectively [34]. N_4 is affected by Sm_2O_3 content in the glassy system under investigation, as seen in the inset figure in Fig. 4. It has been noted that as the Sm_2O_3 content rises the N_4 ratio decreases, indicating that the reduction in BO_4 units is caused by the transformation from BO_4 to BO_3, which raises NBOs. When Sm_2O_3 is added, the boron coordination will probably be converted from 4 to 3. Therefore, the addition of Sm_2O_3 causes a decrease in BO_4 groups. The result is an increase in NBOs in the glassy matrix, which enhances the molar volume, and makes the open structure of the glass system under investigation. This evidence indicates that sm^{3+} ions modify the network in this system [5].

3.4. Optical studies

3.4.1. Band gap and metallization

Fig. 6 (a and b) displays the optical absorption bands and their associated transitions. It exhibits nine absorption bands at 403, 471, 933, 1069, 1219, 1363, 1463, 1526, and 1581 nm. In Table 2, Sm^{3+} ions' transition bands that were observed from the ground state $^6H_{5/2}$ to the excited states $^6P_{3/2}$, $^4I_{11/2}$, $^6F_{11/2}$, $^6F_{9/2}$, $^6F_{7/2}$, $^6F_{5/2}$, $^6F_{3/2}$, $^6H_{15/2}$

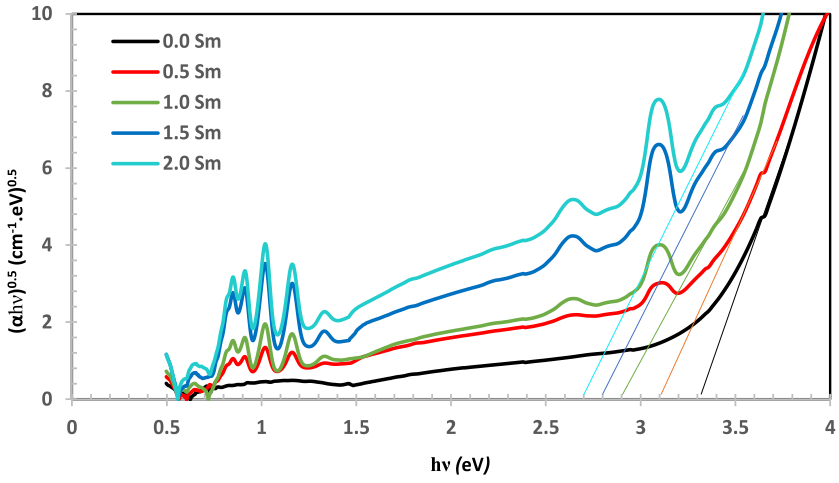

(a)

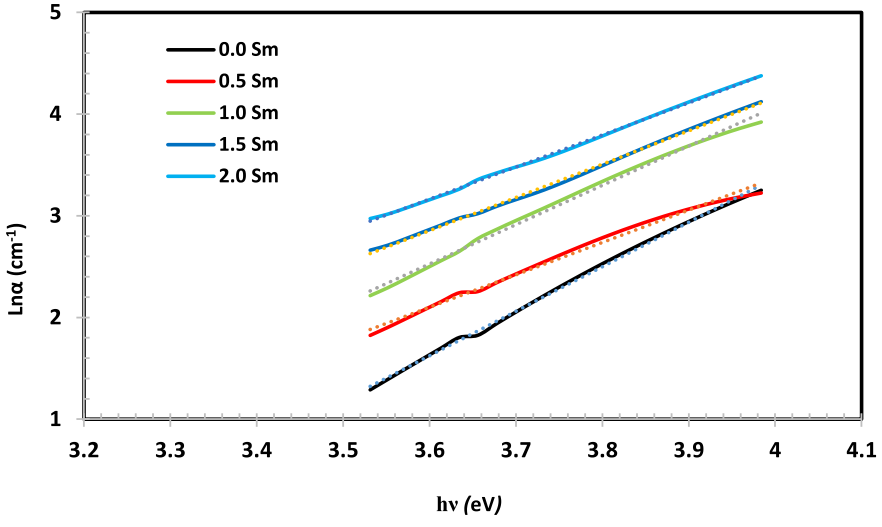

(b)

Fig. 7. (a and b). $(\alpha h\nu)^{1/2}$ and ln α versus photon energy (hν) for all investigated samples, respectively.

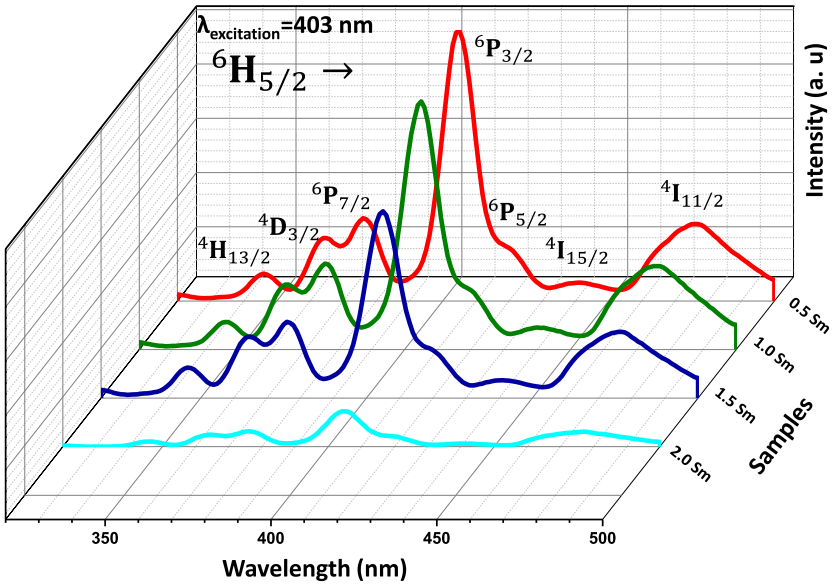

(a)

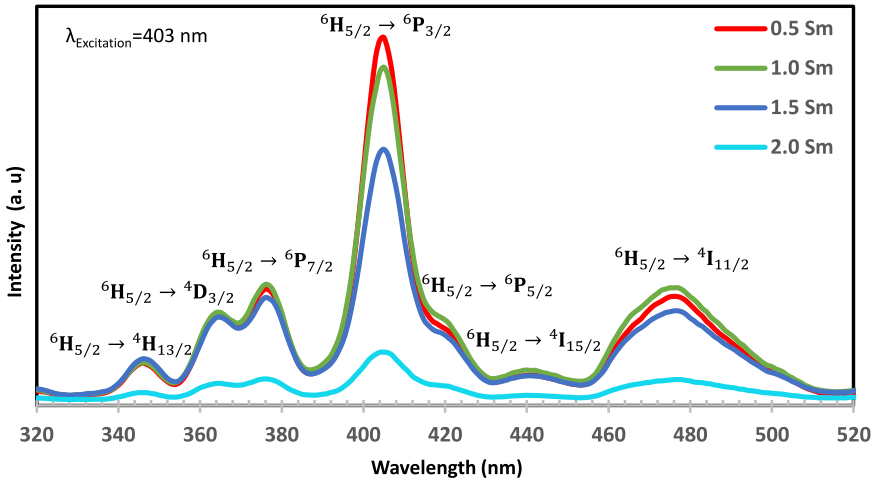

(b)

Fig. 8. (a and b). Excitation spectra of the investigated glassy system.

and $^6F_{1/2}$ [47,48]. The optical absorption spectra provide insight into the electronic band structure of glasses. Variation in band gap concerning glass composition offers essential insights into structural characteristics and bonding features. Tauc's empirical model is employed to estimate E_{opt} [49].

$$\alpha(\nu) = B(h\nu)^{-1}\left(h\nu - E_{opt}\right)^{n} \quad (3)$$

In this equation, B is a constant, while n can take on the values of 2, 3, 1/2, or 1/3 based on the type of transition (indirect or direct). The results indicate an indirect transition of n = 2 for the investigated samples. From Fig. 7 a, E_{opt} values can be estimated. The estimation of the absorption coefficient α(ν) can be achieved by employing (α_0) as a constant, photon energy *hν*, and the Urbach energy ΔE, which signifies the extent of the band tail of localized states that are contained inside the band gap [50,51]:

$$\alpha(\nu) = \alpha_0 \, exp^{\frac{h\nu}{\Delta E}} \quad (4)$$

The estimated values of Eopt, and ΔE are identified in Table 1. The Eopt decreases when Sm_2O_3 is added because the presence of more NBOs in the samples increases disorder, leading to a greater number of localized states and narrower band gaps. The relationship between photon energy (hv) and the natural logarithm of absorption coefficient (lnα) is illustrated in Fig. 7b. The reciprocals of the slopes of the linear portions of the curves were used to determine the Urbach energy (ΔE). With Sm_2O_3 augmentation in glass samples, the Urbach energy increases. This may imply that Sm_2O_3 contributes to increased disorder within glass systems [52].

Furthermore, the metallization criterion (M) represents the mate-

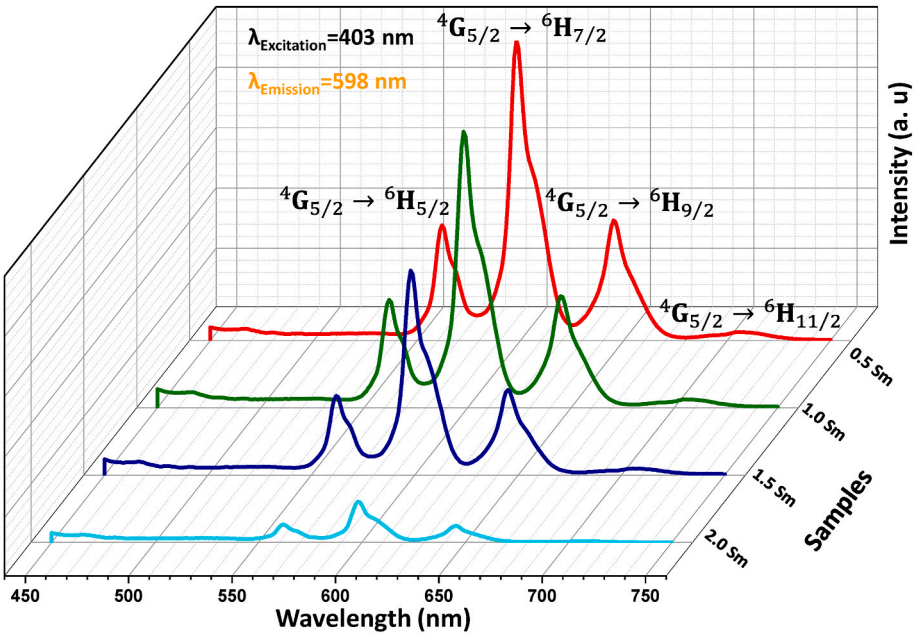

(a)

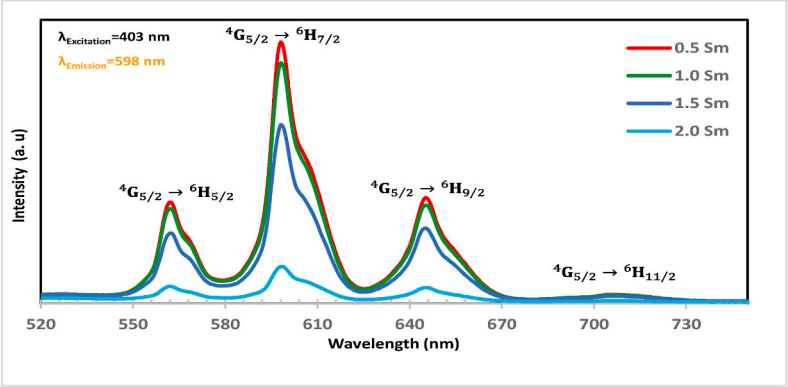

(b)

Fig. 9. (a and b). Emission spectra of the investigated glassy system.

rial's behaviour (insulator, semiconductor, or metallic). The Metallization (M) values for the samples under study can be readily obtained from the Eg values using the Dimitrov and Komatsu formula [53]:

$$M = \sqrt{\frac{E_g}{20}} \tag{5}$$

For the significant values of M, approaching 1, the material exhibits insulating properties. When M is small and close to zero, the material behaves more like a metal because the valence band is in proximity to the conduction band, resulting in a narrow band gap that enhances its metallic character [53]. The M values are decreased for our system, as shown in Table 1 (see Fig. 8).

3.5. Photoluminescence properties

3.5.1. Excitation and emission spectra

Fig. 8 (a and b) displays the excitation spectra of the examined samples. Six distinct bands are depicted in the excitation spectrum. The strongest band observed is at 403 nm ($^6H_{5/2} \rightarrow {}^6P_{3/2}$), serving as a standard for evaluating the produced emission spectra. The emission spectra of Sm_2O_3 at varying concentrations of Sm_2O_3 are displayed in Fig. 9 (a and b) at an excitation wavelength of 403 nm. Four firm peaks within the 520–750 nm range are evident in the transition spectra, which indicate that the $^4G_{5/2} \rightarrow {}^6H_{5/2}$, $^4G_{5/\,2} \rightarrow {}^6H_{7/2}$, $^4G_{5/2} \rightarrow {}^6H_{9/2}$, and $^4G_{5/2} \rightarrow {}^6H_{11/2}$ transitions. These transitions correspond to 562, 598, 646, and 709 nm [54,55].

Glass-doped Sm_2O_3 causes the orange colour due to transitions from the $^4G_{5/2}$ to the $^6H_{7/2}$ and $^6H_{9/2}$ energy levels. The transition to $^6H_{5/2}$ is referred to as the magnetic dipole (MD) and is significantly influenced by the magnetic component of the electromagnetic field. In contrast, the transition to $^6H_{7/2}$ is designated as the electric dipole (ED), which depends only on the electric component of the electromagnetic field and adheres to the selection rules ($\Delta J = \pm 1$) [56]. Solid-state lighting applications utilize these bands, located in the orange and red regions [57]. The simplified schematic in Fig. 10 illustrates the energy levels associated with Sm^{3+} emission.

3.6. Bonding parameters

The slight fluctuation in wavenumbers of rare-earth ions' spectral transition varies from matrix to matrix, causing the nephelauxetic effect [58]. The peak positions are compared with those of the aqua–ion. The

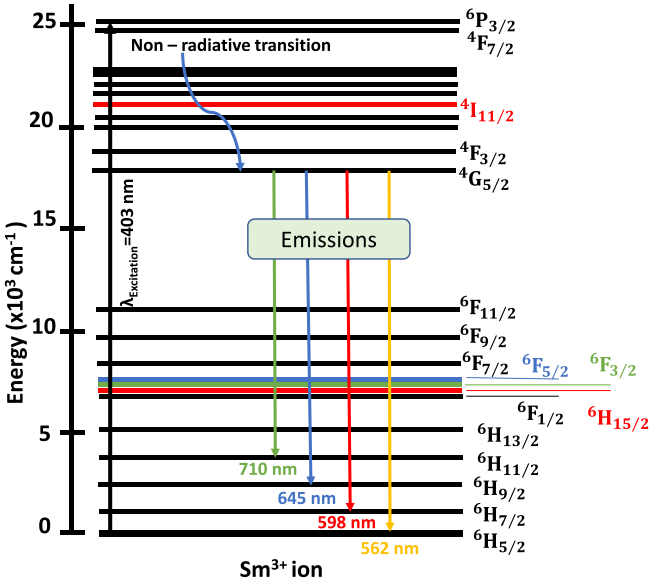

Fig. 10. Simplified schematic representation of energy levels of Sm^{3+} emission.

peak positions are enumerated in Table 3. The nephelauxetic ratio (β) and bonding parameter (δ) can be estimated using the relations [56]:

$$\beta = \frac{V_c}{V_a} \tag{6}$$

where V_a signifies the equivalent wavenumber in the aqueous solution, while V_c denotes the wavenumber associated with the selected transition.

$$\delta = \frac{1 - \overline{B}}{\overline{B}} \tag{7}$$

where $\overline{B}$ is the mean of β, ($\overline{B} = \sum_{NN}^{\beta}$). The parameter δ specifies the bonding interactions of the rare-earth ion with the adjacent ligands. The negative sign represents ionic bonding, and covalent bonding is defined by the positive sign [58]. Table 3 illustrates the formation of ionic bonds between Sm^{3+} ions and their surrounding ligands, highlighting a gradual increase in ionicity.

3.7. Decay curve analysis

A decay curve depicts the relationship between the intensity of emitted light and the time elapsed since activation. It is essential for understanding radiative and non-radiative decay mechanisms and for demonstrating the rate at which Sm^{3+} ions transition from an excited state to a ground state. The decay profiles of the $^4G_{5/2}$ transition of the synthesized Sm^{3+}-doped glassy system, excited at 402 nm and emitting at 598 nm, are illustrated in Fig. 11. The corresponding experimental lifetime (τ_{exp}) values are tabulated in Table 4. A discernible decrease is observed with increasing Sm_2O_3 content. The observed descending

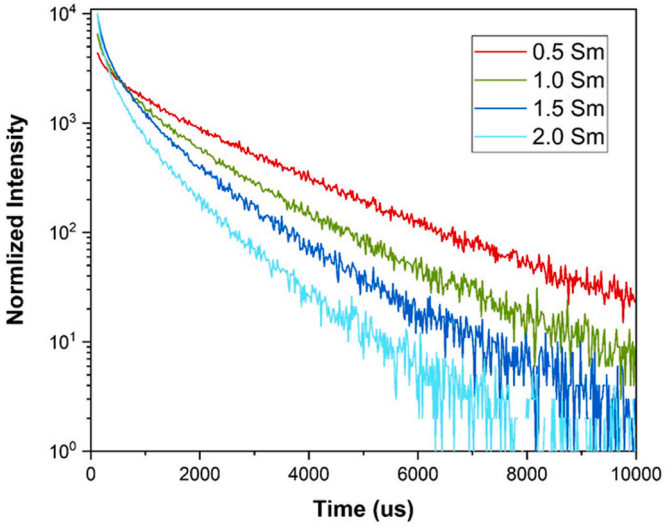

Fig. 11. Decay curves of Sm^{3+} ions doped glassy sestem.

Table 4
Color coordinates (x, y), CCT values (K), Color Purity (Cp), and Average life time decay (ns) of the investigated glasses.

Sample (mol. %)	Color coordinates (x, y)	CCT (K)	(Cp) (%)	Average life time decay (μs)
0.0 Sm	–	–	–	–
0.5 Sm	0.543, 0.405	1860.69	83.86	1.723
1.0 Sm	0.530, 0.402	1919.46	79.94	1.160
1.5 Sm	0.521, 0.401	1970.01	78.33	0.812
2.0 Sm	0.444, 0.389	2759.63	56.65	0.602

Table 3
The transitions, Energy levels (cm^{-1}), along with the wavenumber of the corresponding transition of an aquo-ion ν_{aq}(cm^{-1}), nephelauxetic parameter (β), and bonding parameter (δ) for the investigated glasses.

Transitions $^6H_{5/2}\rightarrow$	ν_{aq} (cm^{-1})	Energy levels (cm^{-1})									
		0.0 Sm		0.5 Sm		1.0 Sm		1.5 Sm		2.0 Sm	
		ν_{Sm} (cm^{-1})	β	ν_{Sm} (cm^{-1})	β	ν_{Sm} (cm^{-1})	β	ν_{Sm} (cm^{-1})	β	ν_{Sm} (cm^{-1})	β
$^6P_{3/2}$	24999	24813	0.9925	24813	0.9925	24813	0.9925	24813	0.9925	24813	0.9925
$^4I_{11/2}$	21096	21231	1.0064	21231	1.0064	21231	1.0064	21231	1.0064	21231	1.0064
$^6F_{11/2}$	10517	10718	1.0191	10706	1.0180	10683	1.0158	10672	1.0147	10660	1.0136
$^6F_{9/2}$	9136	9354	1.0239	9354	1.0239	9354	1.0239	9354	1.0239	9354	1.0239
$^6F_{7/2}$	7977	8203	1.0283	8203	1.0283	8203	1.0283	8203	1.0283	8203	1.0283
$^6F_{5/2}$	7131	7336	1.0288	7336	1.0288	7336	1.0288	7336	1.0288	7336	1.0288
$^6F_{3/2}$	6641	6835	1.0292	6835	1.0292	6835	1.0292	6835	1.0292	6835	1.0292
$^6H_{15/2}$	6508	6553	1.0069	6553	1.0069	6553	1.0069	6553	1.0069	6553	1.0069
$^6F_{1/2}$	6397	6325	0.9887	6325	0.9887	6325	0.9887	6325	0.9887	6325	0.9887
$\overline{\beta}$			1.0138		1.0136		1.0134		1.0133		1.0132
δ			−0.0136		−0.0134		−0.0132		−0.0131		−0.0130

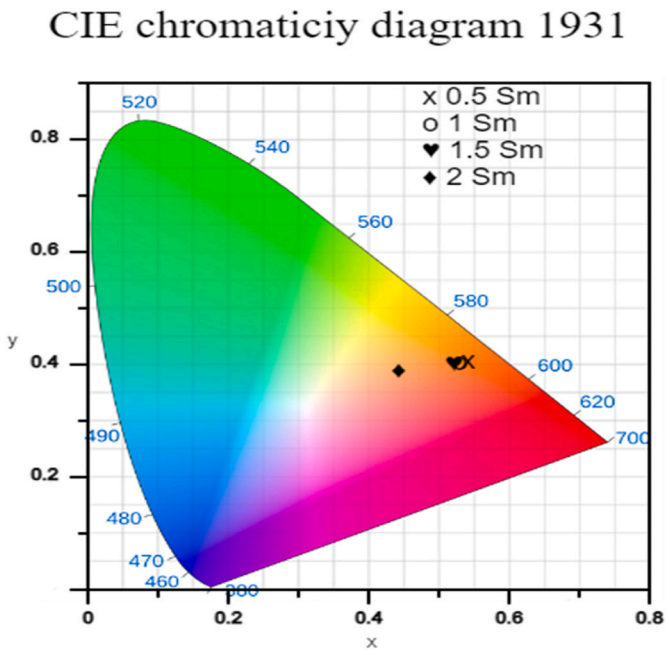

Fig. 12. CIE chromaticity diagram of Sm^{3+} of the investigated glass samples.

order of lifetimes corroborates the energy transfer among the Sm^{3+} ions [59–62].

3.8. CIE diagram

The chromaticity coordinates (x, y) and associated correlated colour temperature (CCT) were established utilizing the Commission International d'Eclairage (CIE) diagram. Consequently, based on the emission spectrum, the quality of the emitted colour was more easily comprehended. To gain a deeper comprehension insight into the characteristics of radiated colour, it is imperative to consider another essential statistical measure, colour purity (CP)%, as outlined in Table 4. The obtained CCT values range from 1860 to 2759 K. Generally, CCT values can be used to distinguish between white and coloured light. Warm emission occurs when the CCT value is less than 3700 K; pure emission occurs when the CCT value is between 3700 and 5000 K, and more excellent emission occurs when the CCT value is more significant than 5000 K for the investigated samples, the CCT values are below the warm CCT range (i.e., CCT<3700 K) [63,64]. McCamy's equation calculates the colour correlated temperature (CCT) [65].

$$CCT = -473\left(\frac{x-0.332}{y-0.186}\right)^2 + 3601\left(\frac{x-0.332}{y-0.186}\right)^2 - 6861\left(\frac{x-0.332}{y-0.186}\right)^2 + 5514.311 \quad (8)$$

For the current samples, the estimated CIE coordinates are located in the reddish–orange emission in the CIE diagram (Fig. 12). The (x, y) chromaticity coordinates, Cp, and CCT indicate that the investigated samples exhibit a bright, warm, luminous colour, making them a promising choice for solid–state lighting applications [66,67].

4. Conclusion

Magnesium-sodium-zinc-borate glasses doped with Sm^{3+} were successfully synthesized. The amorphous nature of the exhibition was confirmed for all glass samples. FT-IR spectroscopy revealed that adding Sm_2O_3 acts as a network modifier, converting BO_4 units to BO_3 units. This process increases the number of non-bridging oxygens (NBOs), leading to a more open, disordered structure. This structural change was directly associated with increases in both density (from 2.50 to 2.68 g/cm^3) and molar volume (from 26.52 to 26.83 cm^3/mol) as the Sm^{3+} content increased. Consequently, the optical band gap (E_{opt}) decreased from 3.39 eV to 2.71 eV with increasing Sm_2O_3 concentration. This results from heightened disorder and the increase in NBOs within the glass network. The Urbach energy (ΔE) also increased, further confirming the increase in structural disorder. The glasses exhibited significant emission in the orange-red region upon excitation at 403 nm. The most prominent peak occurred at 598 nm, matching the $^4G_{5/2} \rightarrow {}^6G_{7/2}$ transition. Additional emission peaks were detected at 562 nm, 646 nm, and 709 nm. The CIE chromaticity coordinates showed that all doped samples emit light in the reddish-orange range. The determined Correlated Colour Temperature (CCT) values varied from 1860 K to 2759 K, placing them in the "warm light" spectrum. The samples, especially the 0.5 mol% Sm^{3+} glass, exhibited a high colour purity of 83.86 %. The efficient orange-red luminescence, favourable warm-light characteristics, and high colour purity indicate that Sm^{3+}-doped borate glasses are strong candidates for applications in orange-red-emitting solid-state lighting, visible lasers, and advanced photonic devices.

CRediT authorship contribution statement

A. Samir: Writing – review & editing, Writing – original draft, Visualization, Methodology, Investigation, Formal analysis, Data curation, Conceptualization. **M. Farouk:** Writing – review & editing, Writing – original draft, Visualization, Validation, Supervision, Methodology, Investigation, Formal analysis, Data curation, Conceptualization. **M. Attallah:** Writing – review & editing, Writing – original draft, Visualization, Validation, Methodology, Investigation, Formal analysis, Data curation, Conceptualization.

Declaration of competing interest

The authors hereby declare that they have no known competing financial interests or other personal relationships, direct or indirect, that could have appeared to influence the work reported in this paper.

References

[1] M.H.A. Mhareb, M.A. Almessiere, M.I. Sayyed, Y.S.M. Alajerami, Optik physical , structural , optical and photons attenuation attributes of lithium-magnesium-borate glasses : role of Tm_2O_3 doping, Optik 182 (2019) 821–831, https://doi.org/10.1016/j.ijleo.2019.01.111.

[2] K. Bansal, P.J. Singh, M. Tyagi, A. Kaur, S. Singh, Physical, structural and spectroscopic studies of Al_2O_3-B_2O_3-Sm_2O_3 scintillating glass doped with heavy metal oxides, J. Lumin. 250 (2022) 119093, https://doi.org/10.1016/j.jlumin.2022.119093.

[3] K. Hanamar, G. Jagannath, S.B. Kolavekar, N.H. Ayachit, H. Patnala, D.A. Aloraini, A.H. Almuqrin, M.I. Sayyed, A.G. Pramod, K. Keshavamurthy, S. Venugopal Rao, B. G. Hegde, Nonlinear optical coefficients of Samarium–activated lithium zinc borate glasses in femtosecond and nanosecond regimes, Opt. Laser Technol. 168 (2024) 109859, https://doi.org/10.1016/j.optlastec.2023.109859.

[4] K. Keshavamurthy, C. Vidya, T. Uthayakumar, V. Hegde, C.M. Joseph, P. Aruna, A. P. Chowdhury, S. Chinnam, K. Gurushantha, C. Devaraja, K. Savanur, S. Malini, B. N. Swetha, Low concentration Sm^{3+} ions loaded zinc sodium borate glasses for solid state lighting devices, Opt. Mater. 148 (2024) 114829, https://doi.org/10.1016/j.optmat.2024.114829.

[5] M.M. Ismail, H.A. Abo-Mosallam, A.G. Darwish, Synthesis, mechanical, and dielectric properties of BaO–CdO–PbO–CeO_2–B_2O_3 glass system through Sm_2O_3 doping for advanced dielectric applications, Ceram. Int. 51 (2025) 25828–25836, https://doi.org/10.1016/j.ceramint.2025.03.267.

[6] M. Farouk, K. Abdallauh, M. Attallah, Z.M.A. El-Fattah, Influence of different alkaline oxide modifiers on VO^{2+} ions doped zinc borate glasses, J. Non-Cryst. Solids 523 (2019) 119607, https://doi.org/10.1016/j.jnoncrysol.2019.119607.

[7] S.N.F. Zalamin, M.H. M Zaid, K.A. Matori, M.K.A. Karim, Y. Yaakob, W.M. Cheong, Z.W. Loh, M.I. Sayyed, Role of Sm3+ ions as network-modifying on elastic, mechanical, and radiation shielding properties of MgO–B_2O_3–TeO_2 glasses, Prog. Nucl. Energy 161 (2023) 104752, https://doi.org/10.1016/j.pnucene.2023.104752.

[8] J.S. Alzahrani, E. Yilmaz, F. Çalişkan, Z.A. Alrowaili, I.O. Olarinoye, M. S. Alqahtani, H. Arslan, M.S. Al-Buriahi, Synthesis and optimization of B2O3-based glass: influence of MgO on hardness, structure properties, and radiation shielding performance, Mater. Today Commun. 37 (2023), https://doi.org/10.1016/j.mtcomm.2023.106933.

[9] H. Liang, X. Liu, J. Tong, P. He, Z. Zhou, Z. Luo, A. Lu, Structure , Judd-Ofelt analysis and spectra studies of Sm^{3+}-doped MO-ZnO-B_2O_3-P_2O_5 (M = Mg , Ca , Sr , Ba) glasses for reddish-orange light application, Ceram. Int. 49 (2023) 15266–15275, https://doi.org/10.1016/j.ceramint.2023.01.110.

[10] M.H.A. Mhareb, Physical , optical and shielding features of - Li_2O – B_2O_3 – MgO – Er_2O_3 glasses co-doped of -Sm_2O_3, Appl. Phys. A 126 (2020) 1–8, https://doi.org/10.1007/s00339-019-3262-9.

[11] O. Bawazeer, M.S. Sadeq, Sm_2O_3 doping-adjusted radiation shielding properties and optical stability under sunlight irradiation of B_2O_3 – Na_2O – Sm_2O_3 – Fe_2O_3 glass, Radiat. Phys. Chem. 217 (2024) 111471, https://doi.org/10.1016/j.radphyschem.2023.111471.

[12] M. Attallah, M. Farouk, A. Samir, Optimize the structural, optical, and thermal properties of Nd^{3+} ions doped boro-aluminum-tungsten glass, Ceram. Int. 50 (2023) 9528–9534, https://doi.org/10.1016/j.ceramint.2023.12.271.

[13] H.M. Elsaghier, A.R. Wassel, M.A. Hassan, S.Y. Marzouk, A. Samir, Impact of ZnO on spectroscopic and luminescence characteristics of Sm_2O_3–SrO–B_2O_3 glasses for warm reddish orange light emitting applications, Mater. Res. Bull. 173 (2024) 112700, https://doi.org/10.1016/j.materresbull.2024.112700.

[14] M. Milanova, L. Aleksandrov, A. Yordanova, R. Iordanova, N.S. Tagiara, A. Herrmann, G. Gao, L. Wondraczek, E.I. Kamitsos, Structural and luminescence behavior of Eu 3 + ions in ZnO-B 2 O 3 -WO_3 glasses, J. Non-Cryst. Solids 600 (2023) 122006, https://doi.org/10.1016/j.jnoncrysol.2022.122006.

[15] M.S. Gaafar, S.Y. Marzouk, I.S. Mahmoud, H.Y. Amin, M.A. Hassan, A. Samir, H. M. Elsaghier, Impact of ZnO on structural, acoustic, and radiation shielding characteristics of B_2O_3-SrO-Sm_2O_3 glasses, Phys. B Condens. Matter 707 (2025) 417183, https://doi.org/10.1016/j.physb.2025.417183.

[16] A.S. Asyikin, A.A. Latif, M.K. Halimah, M.H.M. Zaid, M.A. Kamarudin, M. F. Faznny, S.N. Nazrin, I. Zaitizila, Structural and optical properties of samarium doped silica borotellurite glasses for optical switching application, Opt. Laser Technol. 168 (2024) 109857, https://doi.org/10.1016/j.optlastec.2023.109857.

[17] P. Manyum, W. Rittisut, N. Wantana, Y. Ruangtaweep, N. Srisittipokakun, Green development of samarium borosilicate glasses doped silica gel waste for stable orange colored visible host material, Mater. Today Commun. 38 (2024) 108025, https://doi.org/10.1016/j.mtcomm.2024.108025.

[18] K. Bansal, N. Kumar, I. Abdullahi, P. Jeet, M. Tyagi, S. Singh, Studies of luminescence traits and Judd-Ofelt analysis of Sm^{3+} activated oxyfluoride glasses, Opt. Mater. 147 (2024) 114579, https://doi.org/10.1016/j.optmat.2023.114579.

[19] X. Zhao, S. Xu, L. Wang, Y. Guo, W. Bao, H. Zhang, Thermally stable Dy_2O_3/Sm_2O_3 co-doped glass ceramics containing $La_2Sn_2O_7$ crystal with tunable luminescence, J. Lumin. 266 (2024) 120319, https://doi.org/10.1016/j.jlumin.2023.120319.

[20] M.S. Sadeq, M.S. Alhammad, R. Al-wafi, Effect of samarium oxide on the structural and ligand field parameters of iron cations inside sodium borate glass, Ceram. Int. 50 (2024) 115–125, https://doi.org/10.1016/j.ceramint.2023.10.028.

[21] A. Albekova, K. Jílková, M.H. Míka, Luminescent phosphor glasses with Sm_2O_3 for photodynamic therapy application, Ceram. Int. 51 (2025) 506–511, https://doi.org/10.1016/j.ceramint.2024.11.028.

[22] A. Denprawat, N. Laorodphan, S. Wiltzsch, W. Thiemsorn, Structure modification by Sm_2O_3 substitution for Na_2O to improve properties of alkali zirconium silicate glasses, Ceram. Int. (2025), https://doi.org/10.1016/j.ceramint.2025.06.168.

[23] D. Bayoudhi, C. Bouzidi, E. Matei, M. Secu, A. Catalin, Optical characterization of Sm^{3+} doped phosphate glasses for potential orange laser applications, J. Lumin. 265 (2024) 120204, https://doi.org/10.1016/j.jlumin.2023.120204.

[24] Z. Hong, H. Yue, Z. Lin, X. Luo, H. Hou, S. Wu, F. Lai, W. Wang, W. You, J. Huang, Photoluminescence properties of Dy^{3+}/Sm^{3+} co-doped gallium silicate glass – ceramics for solid-state warm white lighting, J. Non-Cryst. Solids 628 (2024) 122837, https://doi.org/10.1016/j.jnoncrysol.2024.122837.

[25] M.I. Sayyed, D.A. Aloraini, A.H. Almuqrin, S.D. Kamath, Synthesis and characterization of Sm^{3+} doped BaO-ZnO-LiF-B_2O_3 glass system for reddish-orange light generation with high color purity, 155, https://doi.org/10.1016/j.optlastec.2022.108359, 2022.

[26] C.M. Nandanwar, A.N. Yerpude, N.S. Kokode, S.J. Dhoble, Results in Optics Effect of alkali metal ions A^+ (A = K^+ , Na^+ and Li^+) on the photoluminescence properties of Sr_3Bi $(PO_4)_3$: Sm^{3+} phosphors prepared by wet chemical synthesis, Results Opt. (2023) 100456, https://doi.org/10.1016/j.rio.2023.100456, 12.

[27] S.T. Mhashakhetri, A.N. Yerpude, C.M. Nandanwar, A. V Nande, S.J. Dhoble, Investigation of structural , microstructural and optical properties of Ca_3 B_2O_6 : Sm^{3+} downshifting phosphor, Opt. Mater. 165 (2025) 117121, https://doi.org/10.1016/j.optmat.2025.117121.

[28] P.R. Yawale, D.H. Gahane, I.S. Mohurley, Eu $^{3+}$ ion - doped Sr_3Y $(AlO)_3$ $(BO_3)_4$ novel phosphor : synthesis and optical properties, J. Opt. 53 (2024) 4325–4330, https://doi.org/10.1007/s12596-024-01677-5.

[29] D. Aldin, S. Moukhtar, A.H. Zakaria, M.A. El, F.M. Atallah, Optical transitions from hexavalent chromium in lithium - borate glasses, Opt. Quant. Electron. (2021) 1–12, https://doi.org/10.1007/s11082-021-03147-9.

[30] M. Attallah, M. Farouk, A. El-Korashy, M. ElOkr, Copper doped phosphate glass as an optical bandpass filter, Silicon 10 (2018), https://doi.org/10.1007/s12633-016-9488-7.

[31] M. Ehab, E. Salama, A. Ashour, M. Attallah, Optical properties and gamma radiation shielding capability of transparent barium borosilicate glass composite, Sustainability 14 (2022) 13298.

[32] M. Farouk, H.M. Mokhtar, Z.M.A. El-fattah, A. Samir, Vanadyl doped Li-zinc borate glasses : optical and ESR study, J. Non-Cryst. Solids 568 (2021) 120964, https://doi.org/10.1016/j.jnoncrysol.2021.120964.

[33] E.A. Elkelany, M.A. Hassan, A. Samir, A.M. Abdel-ghany, H. El-bahnasawy, M. Farouk, Ssbauer spectroscopy of lithium tetraborate glass doped Optical and M o with iron oxide, Opt. Mater. 112 (2021) 110744, https://doi.org/10.1016/j.optmat.2020.110744.

[34] M. Farouk, A. Samir, F. Metawe, M. Elokr, Optical absorption and structural studies of bismuth borate glasses containing Er^{3+} ions, J. Non-Cryst. Solids 371–372 (2013) 14–21, https://doi.org/10.1016/j.jnoncrysol.2013.04.001.

[35] H.Y. Morshidy, M.S. Sadeq, In fl uence of cobalt ions on the structure , phonon emission , phonon absorption and ligand fi eld of some sodium borate glasses, J. Non-Cryst. Solids 525 (2019) 119666, https://doi.org/10.1016/j.jnoncrysol.2019.119666.

[36] M.A. Marzouk, F.H. Elbatal, H.A. Elbatal, Effect of TiO_2 on the optical , structural and crystallization behavior of barium borate glasses, Opt. Mater. 57 (2016) 14–22, https://doi.org/10.1016/j.optmat.2016.04.002.

[37] A.M. Abdelghany, M.A. Ouis, M.A. Azooz, H.A. Elbatal, G.T. El-bassyouni, Spectrochimica Acta part A : molecular and biomolecular spectroscopy role of SrO on the bioactivity behavior of some ternary borate glasses and their glass ceramic derivatives, Spectrochim. ACTA PART A Mol. Biomol. Spectrosc. 152 (2016) 126–133, https://doi.org/10.1016/j.saa.2015.07.072.

[38] K.N. Sharvani, G. Prasad S, J. Kaewkhao, N. Intachai, S. Kothan, W. Rachniyom, A. Pasha, R. Rajaramakrishna, Optical and structural properties of Eu^{3+} doped MgO–Li_2O–Na_2O–BaO–B_2O_3 glasses for scintillating glass applications, Radiat. Phys. Chem. 199 (2022), https://doi.org/10.1016/j.radphyschem.2022.110295.

[39] H.Y. Morshidy, A.R. Mohamed, A.A. Abul-magd, M.A. Hassan, Role of high energy Cr^{6+} optical transition induced by rare earth ion (La^{3+}) in compositional-dependent borate glass, Mater. Chem. Phys. 289 (2022) 126503, https://doi.org/10.1016/j.matchemphys.2022.126503.

[40] M. Farouk, D.-A. Slibi, Z.M. Abd El-Fattah, M. Atallah, M.A. El-Sherbiny, M. A. Hassan, Effect of SiO_2 addition on chromium transitions in borate glasses, Silicon 13 (2021) 3003–3010, https://doi.org/10.1007/s12633-020-00649-1.

[41] E.I. Kamitsos, A.P. Patsis, M.A. Karakassides, G.D. Chryssikos, Infrared reflectance spectra of lithium borate glasses, J. Non-Cryst. Solids 126 (1990) 52–67, https://doi.org/10.1016/0022-3093(90)91023-K.

[42] H.Y. Morshidy, Z.M.A. El-fattah, A.A. Abul-magd, M.A. Hassan, A.R. Mohamed, Reevaluation of Cr^{6+} optical transitions through Gd_2O_3 doping of chromium-borate glasses, 113, https://doi.org/10.1016/j.optmat.2021.110881, 2021.

[43] M. Abo, A. Saeed, R.M. El Shazly, H.M.E. Mallah, E. Elesh, Optik double effect of glass former B_2O_3 and intermediate Pb_3O_4 augmentation on the structural , thermal , and optical properties of borate network, Optik 272 (2023) 170368, https://doi.org/10.1016/j.ijleo.2022.170368.

[44] I.E. Kotb, A. Okasha, S.Y. Marzouk, N.A. Zidan, Extensive study on the optical and structural characteristics of Nd^{3+} doped lead-borate-strontium-tungsten glass system: Judd–Ofelt analysis, Results Chem (2023) 100869, https://doi.org/10.1016/J.RECHEM.2023.100869, 5.

[45] A.A. Abul-Magd, H.Y. Morshidy, A.M. Abdel-Ghany, The role of NiO on the structural and optical properties of sodium zinc borate glasses, Opt. Mater. 109 (2020), https://doi.org/10.1016/j.optmat.2020.110301.

[46] F. Ahmad, Study the effect of alkali/alkaline earth addition on the environment of borochromate glasses by means of spectroscopic analysis, J. Alloys Compd. 586 (2014) 605–610, https://doi.org/10.1016/j.jallcom.2013.10.105.

[47] A. Ratep, I. Kashif, Luminescence characteristics of bismuth borate glass doped with different rare earth AO (A = Ce, Nd, Sm), Radiat. Phys. Chem. 237 (2025) 113095, https://doi.org/10.1016/j.radphyschem.2025.113095.

[48] G. Dedeepya, S. Mahamuda, V. Balaji, E.O. Echeweozo, A.S. Rao, M.S. Al-Buriahi, Sm^{3+} ions doped titanium borate glasses: a study on structural, optical & radiation shielding properties, Nucl. Instrum. Methods Phys. Res. Sect. B Beam Interact. Mater. Atoms 566 (2025) 165792, https://doi.org/10.1016/j.nimb.2025.165792.

[49] N.S. Anad, Z.M.A. El-Fattah, M. Attallah, H.M. Ahmed, M.M. El-Okr, H.H. El-Bahnasawy, Precise determination of optical band gap in Cr-doped semiconductor nanowires, Opt. Quant. Electron. 54 (2022), https://doi.org/10.1007/s11082-021-03462-1.

[50] M.F.A. Samir, A.I.M.A. Farag, Raman , FTIR studies and optical absorption of zinc borate glasses containing - WO_3, Appl. Phys. A 126 (2020) 1–8, https://doi.org/10.1007/s00339-020-03890-y.

[51] A. Samir, Influence of Na_2O addition on the alkali borochromate glasses: structure and ligand field, Indian J. Phys. 95 (2021) 2169–2175, https://doi.org/10.1007/s12648-020-01842-z.

[52] C. Rajyasree, S. Bala Murali Krishna, A. Ramesh Babu, D. Krishna Rao, Structural impact of cobalt ions on $BaBiBO_4$ glass system by means of spectroscopic and dielectric studies, J. Mol. Struct. 1033 (2013) 200–207, https://doi.org/10.1016/j.molstruc.2012.08.040.

[53] M.I. Sayyed, M.A. Abdo, H.E. Ali, H.A. Ahmed, M.S. Sadeq, Optik Impact of lead oxide on the structure , optical , and radiation shielding properties of potassium borate glass doped with samarium ions, Optik 278 (2023) 170738, https://doi.org/10.1016/j.ijleo.2023.170738.

[54] G. Dedeepya, S. Mahamuda, K. Swapna, M. Venkateswarlu, A.S. Rao, Optical response characteristics & radiation shielding properties of Sm^{3+} ions activated tungsten alkali borate glasses for visible laser & radiation shielding applications, Solid State Sci. 163 (2025) 107888, https://doi.org/10.1016/j.solidstatesciences.2025.107888.

[55] C.M. Nandanwar, N.S. Kokode, R.M. Yerojwar, A.N. Yerpude, Nano-structures & nano-objects combustion synthesis and photoluminescence study of novel Sm^{3+} activated K_3La $(PO_4)_2$ phosphor for n-UV solid state lighting, Nano-Struct. Nano-Objects 36 (2023) 101068, https://doi.org/10.1016/j.nanoso.2023.101068.

[56] A. Ichoja, S. Hashim, S.K. Ghoshal, Unique optical traits of Sm^{3+}-doped magnesium borate glass, Chinese, J. Phys. 66 (2020) 36–49, https://doi.org/10.1016/j.cjph.2020.05.010.

[57] J. Dahiya, A. Hooda, A. Agarwal, S. Khasa, Effect of dysprosium and samarium RE ion Co-doping on photoluminescence behaviour of novel alkali fluoride bismuth borate glasses : a white LED material, Opt. Mater. 134 (2022) 113162, https://doi.org/10.1016/j.optmat.2022.113162.

[58] N.S. Prabhu, A.N. Meza-Rocha, O. Soriano-Romero, U. Caldiño, E.F. Huerta, C. Falcony, M.I. Sayyed, H. Al-Ghamdi, A.H. Almuqrin, S.D. Kamath, Spectroscopic study of Er^{3+} doped borate glass system for green emission device, NIR laser, and optical amplifier applications, J. Lumin. 238 (2021), https://doi.org/10.1016/j.jlumin.2021.118216.

[59] G. Dedeepya, S. Mahamuda, V. Balaji, E.O. Echeweozo, A.S. Rao, M.S. Al-buriahi, Nuclear inst . and methods in physics research , B Sm^{3+} ions doped titanium borate glasses : a study on structural, optical & radiation shielding properties, Nucl. Instrum. Methods Phys. Res. B 566 (2025) 165792, https://doi.org/10.1016/j.nimb.2025.165792.

[60] B.N. Swetha, A. Paul, M.K. Kokila, Sodium lanthanum boro-tellurite glasses with Sm^{3+} ion doping and gold nanoparticle embedding : a new glass matrix for solid state lighting devices, J. Alloys Compd. 1010 (2025) 177628, https://doi.org/10.1016/j.jallcom.2024.177628.

[61] R. Rajaramakrishna, N. Nikolay, N. Wantana, H.J. Kim, S. Kothan, N. Intachai, W. Busayaporn, J. Kaewkhao, E. V Parfenova, A.S. Aleksandrovsky, Quantum yield , energy transfer , and x-ray induced study of Sm^{3+} ions doped oxide glasses for intense orange-red photo-emitting optoelectronic device applications, Chem. Phys. 590 (2025) 112528, https://doi.org/10.1016/j.chemphys.2024.112528.

[62] Y. Zhang, X. Deng, R. Cui, X. Guo, J. Zhang, C. Deng, A novel single-phase $Ca_3Gd_2Si_3O_{12}$: Dy^{3+}, Sm^{3+} phosphor exhibiting high thermal stability for solid-state lighting applications, Ceram. Int. 51 (2025) 31466–31477, https://doi.org/10.1016/j.ceramint.2025.04.336.

[63] D. Garima, V. Hebbar, B. Gurav, J. Kaewkhao, N. Intachai, S. Kothan, R. Rajaramakrishna, Optical properties of Sm^{3+} doped in $CaO\text{-}Al_2O_3\text{-}Na_2O\text{-}BaO\text{-}B_2O_3$ glasses for under-sea optical device applications, Optik 262 (2022) 169366, https://doi.org/10.1016/j.ijleo.2022.169366.

[64] S. Hemalatha, M. Nagaraja, A. Madhu, N. Srinatha, J. Ofelt, Results in optics rare Earth (Dy^{3+}-ion) induced near white light emission in sodium-zinc-borate glasses, Results Opt 9 (2022) 100275, https://doi.org/10.1016/j.rio.2022.100275.

[65] H.M. Elsaghier, M.A. Azooz, N.A. Zidan, W. Abbas, A. Okasha, S.Y. Marzouk, Spectroscopic and optical investigations on Er^{3+} ions doped alkali cadmium phosphate glasses for laser applications, J. Non-Cryst. Solids 588 (2022) 121616, https://doi.org/10.1016/j.jnoncrysol.2022.121616.

[66] R.M. Yerojwar, N.S. Kokode, C.M. Nandanwar, Synthesis and photoluminescence properties of - $CaMgAl_{10}O_{17}$: Sm^{3+} phosphor for n-UV solid-state lighting, J. Opt. 53 (2024) 4423–4428, https://doi.org/10.1007/s12596-023-01611-1.

[67] D.M. Parshuramkar, A.N. Yerpude, C.M. Nandanwar, S.J. Dhoble, Photoluminescence properties of $CaMgB_2O_5$: RE^{3+} (RE = Dy , Eu , Sm) environmental friendly phosphor for solid state lighting, Indian J. Phys. 98 (2024) 1977–1983, https://doi.org/10.1007/s12648-023-02966-8.